

# Toroidal Crystals

Luca Giomi and Mark J. Bowick

Department of Physics, Syracuse University, Syracuse New York, 13244-1130

Crystalline assemblages of identical sub-units packed together and elastically bent in the form of a torus have been found in the past ten years in a variety of systems of surprisingly different nature, such as viral capsids, self-assembled monolayers and carbon nanomaterials. In this Letter we analyze the structural properties of toroidal crystals and we provide a unified description based on the elastic theory of defects in curved geometries. We find ground states characterized by the presence of 5-fold disclinations on the exterior of the torus and 7-fold disclinations in the interior. The number of excess disclinations is controlled primarily by the aspect ratio of the torus, suggesting a novel mechanism for creating toroidal templates with precisely controlled valency via functionalization of the defect sites.

Toroidal micelles can be formed in the self-assembly of dumbbell-shaped amphiphilic molecules [1]. Molecular dumbbells dissolved in a selective solvent self-assemble in aggregate structures determined by their amphiphilic character. This process yields coexisting spherical and open-ended cylindrical micelles which evolve slowly over the course of a week to more stable toroidal micelles. Toroidal geometries also occur in microbiology in the viral capsid of the coronavirus *torovirus* [2]. The torovirus is an RNA viral package of maximal diameter between 120 and 140 nm and is surrounded, as other coronaviridae, by a double wreath/ring of cladding proteins.

Carbon nanotori form another fascinating and technologically promising class of toroidal crystals [3] with remarkable magnetic and electronic properties. The interplay between the ballistic motion of the  $\pi$  electrons and the geometry of the embedding torus leads to a *colossal* paramagnetic moment in metallic carbon tori [4]. The high magnetic susceptibility, together with large ring radius (up to  $0.03 \mu\text{m}$  for single tubes of 1.4 nm in diameter [5]), implies that the mobility of the electrons in the highest occupied molecular orbital is several times larger than that of other ring-shaped molecules such as benzene [6].

A unified theoretical framework to describe the structure of toroidal crystals is provided by the elastic theory of defects in a curved background [7, 8, 9, 10]. This formalism has the advantage of far fewer degrees of freedom than a direct treatment of the microscopic interactions and allows one to explore the origin of the emergent symmetry observed and expected in toroidal crystals as the result of the interplay between defects and geometry. Since defective regions are natural places for biological activity and chemical linking, a thorough understanding of the surface topology of crystalline assemblages could represent a significant step toward a first-principle design of entire libraries of nano and mesoscale components with precisely determined valency that could serve as the building blocks for mesomolecules or bulk materials via self-assembly or controlled fabrication.

The embedding of an equal number of pentagonal and heptagonal disclination defects in a hexagonal carbon network was first proposed by Dunlap in 1992 as a pos-

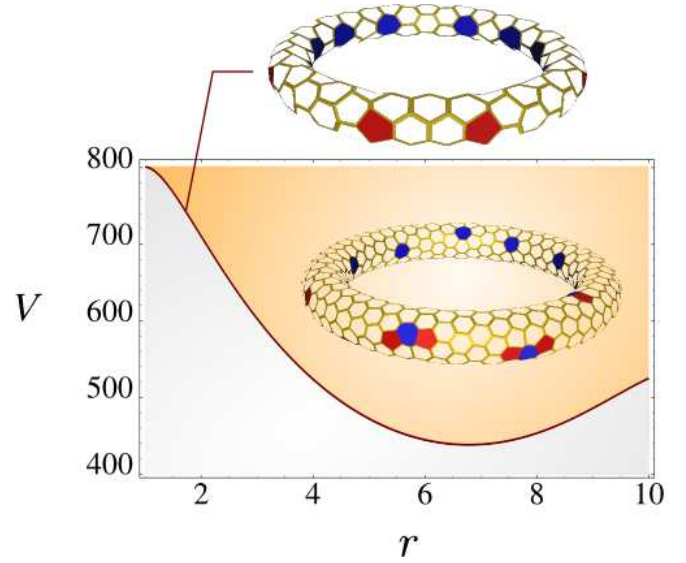


FIG. 1: (Color online) Isolated defects and scar phases in the  $(r, V)$  plane. When the number of vertices  $V$  increases the range of the screening curvature becomes smaller than one lattice spacing and disclinations appear delocalized in the form of a 5 – 7 – 5 grain boundary mini-scar.

sible way to incorporate positive and negative Gaussian curvature into the cylindrical geometry of nanotubes [11]. In the Dunlap construction the curvature is achieved by the insertion of “knees” in conjunction with each pentagon-heptagon pair arising from the junction of tubular segments of different chirality. The latter is conventionally specified by two integers  $(N, M)$  which identify the direction along which a planar triangular lattice is rolled up in the form of a tube [12]. A junction between an  $(N, 0)$  and an  $(N, N)$  tube is obtained, for instance, by placing a 7-fold disclination along the internal equator of the torus and a 5-fold disclination along the external equator [13, 14]. By repeating the 5 – 7 connection periodically it is possible to construct an infinite number of toroidal lattices with an even number of disclinations pairs and the dihedral symmetry group  $D_{nh}$  (where  $2n$  is the total number of 5 – 7 pairs).

Another class of crystalline toroids with dihedral antiprismatic symmetry  $D_{nd}$  was initially proposed by Itoh *et al* [15] shortly after Dunlap. Aimed at producing a structure similar to  $C_{60}$  fullerene, Itoh's original construction implied ten disclination pairs and the symmetry group  $D_{5d}$ . In contrast to Dunlap toroids, the disclinations in the antiprismatic torus are not perfectly aligned along the equator but rather staggered at some angular distance  $\delta\psi$  from the equatorial plane. A general classification scheme for  $D_{nd}$  symmetric tori can be found in Ref. 16. In this paper we will refer to the lattices themselves, with  $2n$  disclination pairs, by the symbols  $TPn$  and  $TAn$ , with respective symmetry groups  $D_{nh}$  and  $D_{nd}$ .

Within the elastic theory of defects on curved surfaces [7, 8, 9, 10] the original interacting particle problem is mapped to a system of interacting disclination defects in a continuum elastic curved background. Disclinations are characterized by their topological or disclination charge,  $q_i$ , representing the departure of a vertex from a perfect triangular lattice. Thus  $q_i = 6 - c_i$ , where  $c_i$  is the coordination number of the  $i$ th vertex. A classic theorem of Euler requires the total disclination charge of any triangulation of a two-dimensional manifold  $M$  to be equal to  $6\chi_M$ , where  $\chi_M$  is the Euler characteristic of  $M$ . In the case of the torus  $\chi_M = 0$ , and thus disclinations must appear in pairs of opposite disclination charge (i.e. 5-fold and 7-fold vertices with  $q_i = 1$  and  $-1$  respectively) in order to ensure disclination charge neutrality. The total free energy of a toroidal crystal with  $N$  disclinations can be expressed as

$$F_{el} = \frac{1}{2Y} \int_M d^2x \Gamma^2(\mathbf{x}) + \epsilon_c \sum_{i=1}^N q_i^2 + F_0, \quad (1)$$

where  $Y$  is the 2D-Young modulus and  $\Gamma(\mathbf{x})$  is the solution of the following Poisson problem with periodic boundary conditions:

$$\Delta \Gamma(\mathbf{x}) = Y \rho(\mathbf{x}), \quad (2)$$

where  $\Delta$  is the Laplace-Beltrami operator on the torus and  $\rho(\mathbf{x})$  is the total topological charge density

$$\rho(\mathbf{x}) = \frac{\pi}{3} \sum_{k=1}^N q_k \delta(\mathbf{x}, \mathbf{x}_k) - K(\mathbf{x}) \quad (3)$$

of  $N$  disclinations located at the sites  $\mathbf{x}_k$  plus a screening contribution due to the Gaussian curvature  $K(\mathbf{x})$  of the embedding manifold. The first term in Eq. (1) represents the long-range elastic distortion due to defects and curvature. Its form resembles the potential energy of a system of electrical charges. In this analogy the Gaussian curvature  $K(\mathbf{x})$  plays the role of a non-uniform background charge distribution while defects appear as positively and negatively charged point-like particles. As

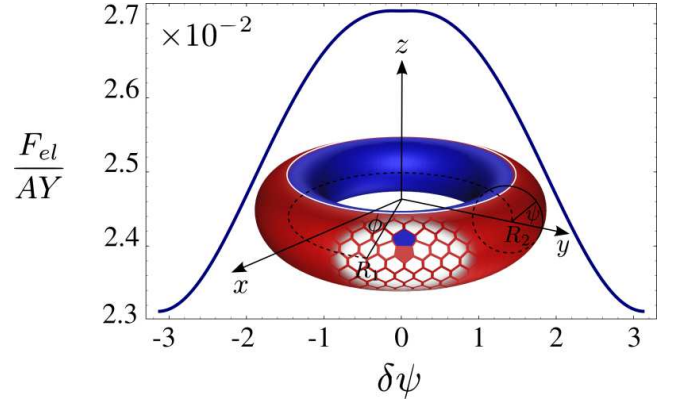


FIG. 2: (Color online) Elastic energy of a 5 – 7 disclination dipole constrained to lie on the same meridian, as a function of the angular separation. In the inset, illustration of a circular torus of radii  $R_1 > R_2$ . Regions of positive and negative Gaussian curvature have been shaded in red and blue respectively. A standard parametrization of the torus is obtained by considering the angles  $\psi$  and  $\phi$ .

a result, disclinations arrange themselves so to approximately match the Gaussian curvature. The second term in Eq. (1) is the defect core-energy representing the energy required to create a single disclination defect. This quantity is related to the short-distance cut-off of the elastic theory and is proportional to the square of the topological charge times a constant  $\epsilon_c$ . Finally  $F_0$  is an offset corresponding to the free energy of a flat defect-free monolayer.

Using standard analysis the function  $\Gamma(\mathbf{x})$  can be written in the form

$$\Gamma(\mathbf{x}) = \frac{\pi}{3} \sum_{k=1}^N q_k \Gamma_d(\mathbf{x}, \mathbf{x}_k) - \Gamma_s(\mathbf{x}), \quad (4)$$

where  $\Gamma_s(\mathbf{x})$  represents the stress field due to the curvature of the torus and is given by:

$$\frac{\Gamma_s(\mathbf{x})}{Y} = \log \left[ \frac{r + \sqrt{r^2 - 1}}{2(r + \cos \psi)} \right] + \frac{r - \sqrt{r^2 - 1}}{r}, \quad (5)$$

where  $r = R_1/R_2$  is the aspect ratio of the torus. The function  $\Gamma_d(\mathbf{x}, \mathbf{x}_k)$  is the stress field at the point  $\mathbf{x}$  arising from the elastic distortion due to a defect at  $\mathbf{x}_k$  and is given by

$$\begin{aligned} \frac{\Gamma_d(\mathbf{x}, \mathbf{x}_k)}{Y} &= \frac{\kappa}{16\pi^2} \left( \psi_k - \frac{2}{\kappa} \xi_k \right)^2 - \frac{1}{4\pi^2 \kappa} (\phi - \phi_k)^2 \\ &+ \frac{1}{4\pi^2 r} \log(r + \cos \psi_k) - \frac{\kappa}{4\pi^2} \text{Re}\{\text{Li}_2(\alpha e^{i\psi_k})\} \\ &+ \frac{1}{2\pi} \log \left| \vartheta_1 \left( \frac{z - z_k}{\kappa} \middle| \frac{2i}{\kappa} \right) \right|, \end{aligned} \quad (6)$$

where  $\xi = \kappa \tan^{-1}(\omega \tan \psi/2)$  is a conformal angle arising from the mapping of the torus to the periodic plane,

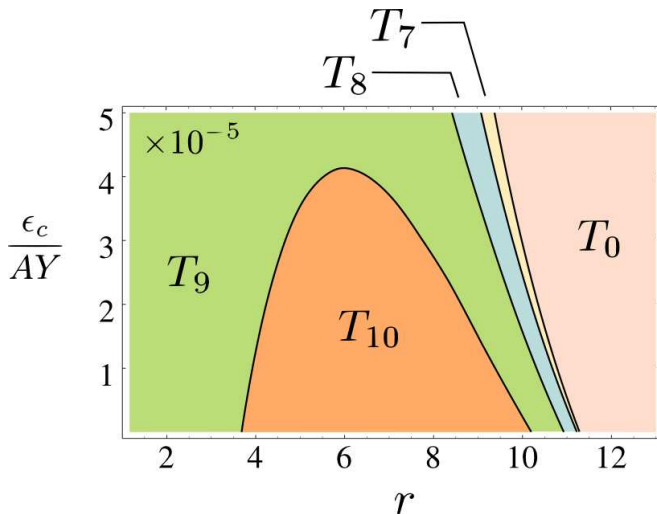


FIG. 3: (Color online) Phase diagram for  $T_p$  configurations in the plane  $(r, \epsilon_c / AY)$ . For  $r \in [3.68, 10.12]$  and  $\epsilon_c \sim 0$  the structure is given by a  $T_{10}$  configuration with symmetry group  $D_{5h}$ .

$z = \xi + i\phi$ , and  $\alpha$ ,  $\kappa$  and  $\omega$  are dimensionless constants depending on the aspect ratio  $r$ :

$$\alpha = \sqrt{r^2 - 1} - r, \quad \kappa = \frac{2}{\sqrt{r^2 - 1}}, \quad \omega = \sqrt{\frac{r-1}{r+1}}.$$

Finally  $\vartheta_1$  is a Jacobian theta function and reflects the double periodicity of the torus [17].

To analyze the elastic energy Eq. (1) we first consider the simplest case of two opposite sign disclinations lying on the same meridian of a torus of area  $A = 4\pi^2 R_1 R_2$ . The elastic free energy of this system is shown in Fig. 2 as a function of the angular separation between the two disclinations. The minimum is obtained for the positive disclination along the external equator of the torus (where  $K(\mathbf{x})$  is maximally positive) and the negative disclination along the internal equator (where  $K(\mathbf{x})$  is maximally negative). The picture emerging from this simple case suggests a procedure to systematically construct optimal defect patterns for an arbitrary number of disclination pairs, by placing the same number of equally spaced  $+1$  and  $-1$  disclinations along the internal and external equators respectively. We name this configuration with the symbol  $T_p$ , where  $p$  stands for the total number of disclination dipoles.

A comparison between the free energy of different  $T_p$  configurations as a function of aspect ratio and core energy is summarized in the phase diagram of Fig. 3. We stress here that only  $T_p$  graphs with  $p$  even have an embedding on the torus corresponding to lattices of the  $TP_2^p$  class. Nevertheless a comparison with  $p$ -odd configurations can provide additional information regarding the stability of  $p$ -even lattices. The defect core energy entering Eq. (1) is equal to  $2p\epsilon_c$ . Although dependent

on the microscopic details of the system, the constant  $\epsilon_c / AY \sim 10^{-5}$  for a crystal of roughly  $10^3$  atoms. In the range  $r \in [3.68, 10.12]$  and  $\epsilon_c \sim 0$ , the structure is dominated by the  $T_{10}$  phase corresponding to a double ring of  $+1$  and  $-1$  disclinations distributed along the external and internal equators of the torus at the vertices of a regular decagon. The corresponding lattice has  $D_{5h}$  symmetry group.

That this structure might represent a stable configuration for polygonal carbon toroids has been conjectured by the authors of Ref. 13, based on the argument that the  $36^\circ$  angle arising from the insertion of ten pentagonal-heptagonal pairs into the lattice would optimize the geometry of a nanotorus consistently with the structure of the  $sp^2$  bonds of the carbon network (unlike the  $30^\circ$  angle of the 6-fold symmetric configuration originally proposed by Dunlap). In later molecular dynamics simulations, Han [18] found that a 5-fold symmetric lattice, such as the one obtained from a  $(9,0)/(5,5)$  junction, is in fact stable for toroids with aspect ratio less than  $r \sim 10$ . The stability, in this case, results from the strain energy per atom being smaller than the binding energy of carbon atoms. We have shown here, from first principles, that a 5-fold symmetric lattice indeed constitutes a minimum of the elastic energy for a broad range of aspect ratios and defect core energies.

For small aspect ratios the 5-fold symmetric configuration becomes unstable and is replaced by the  $T_9$  phase. This configuration, however, does not correspond to a possible triangulation of the torus. In this regime, we expect the minimal energy structure to consist of ten non-coplanar disclination pairs as in the antiprismatic

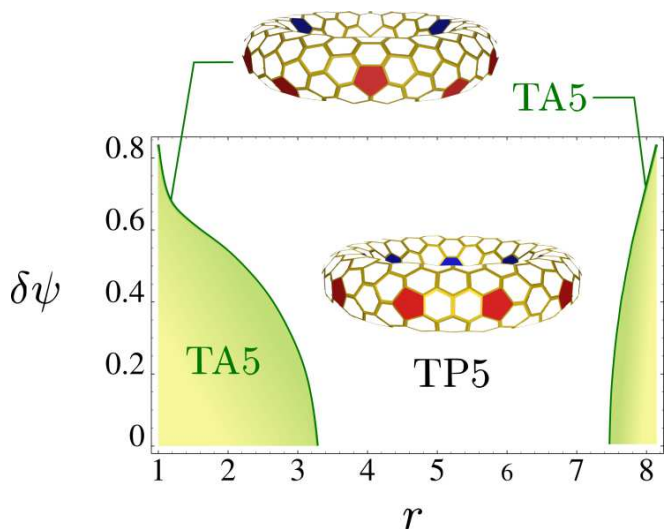


FIG. 4: (Color online) Phase diagram of a 5-fold symmetric lattice in the plane  $(r, \delta\psi)$ . For small  $\delta\psi$  and  $r$  in the range  $[3.3, 7.5]$  the prismatic  $TP5$  configuration is energetically favored. For  $r < 3.3$ , the system undergoes a structural transition to the antiprismatic phase  $TA5$ .

TA5 lattice. The latter can be analyzed by introducing a further degree of freedom,  $\delta\psi$ , representing the angular displacement of defects from the equatorial plane. A comparison between the TP5 and TA5 configurations is shown in Fig. 4 for different values of  $\delta\psi$ . For small  $\delta\psi$  and  $r \in [3.3, 7.5]$  the prismatic TP5 configuration is energetically favored. For  $r < 3.3$ , however, the lattice undergoes a structural transition to the TA5 phase. For  $r > 7.5$  the prismatic symmetry of the TP5 configuration breaks down again. In this regime, however, the elastic energy of both configurations rapidly becomes higher because of the lower curvature and defects disappear.

In the regime of large particle numbers, the amount of curvature required to screen the stress field of an isolated disclination in units of lattice spacing becomes too large and disclinations are unstable to grain boundary “scars” consisting of a linear array of tightly bound 5 – 7 pairs radiating from an unpaired disclination [8, 10]. In a manifold with variable Gaussian curvature this process yields the coexistence of isolated disclinations (in regions of large curvature) and scars. In the case of the torus the Gaussian curvature in the interior is always larger in magnitude than that in the exterior for any  $R_1 > R_2$  and thus we may expect a regime in which the negative internal curvature is still large enough to support the existence of isolated 7-fold disclinations, while on the exterior of the torus disclinations are delocalized in the form of positively charged grain boundary scars.

To check this hypothesis we compare the energy of the TP5 lattice previously described with that of “scarred” configurations obtained by decorating the original toroid in such a way that each pentagonal disclination on the external equator is replaced by a 5 – 7 – 5 scar. The result of this comparison is summarized in the phase diagram of Fig. 1 in terms of  $r$  and the number of vertices of the triangular lattice  $V$  (the corresponding hexagonal lattice has twice the number of vertices, i.e.  $V_{hex} = 2V$ ).  $V$  can be derived from the angular separation of neighboring disclinations in the same scar by approximating  $V \approx A/A_V$ , with  $A_V = \frac{\sqrt{3}}{2}a^2$  the area of a hexagonal Voronoi cell and  $a$  the lattice spacing. When the aspect ratio is increased from 1 to 6.8 the range of the curvature screening becomes shorter and the number of atoms required to destroy the stability of the TP5 lattice decreases. For  $r > 6.8$ , however, the geodesic distance between the two equators of the torus becomes too small and the repulsion between like-sign defects takes over. Thus the trend is inverted.

On the material science side, defects can be functionalized to provide binding sites for ligands. The number of excess disclinations will then determine the valency of the surface, which itself can serve as a building block for new molecules and bulk materials [19]. The universality of the predictions presented here means that one has precise

control of the valency by tuning the aspect ratio of the torus. This could lead to a very efficient scheme for creating a variety of basic surfaces with well-defined valency which subsequently self-assemble into novel molecules and bulk structures.

We acknowledge David Nelson and Alex Travesset for stimulating discussions. This work was supported by the NSF through Grant No. DMR-0219292 (ITR) and by an allocation through the TeraGrid Advanced Support Program.

- 
- [1] J. K. Kim, E. Lee, Z. Huang and M. Lee, J. Am. Chem. Soc. **128**, 14022 (2006).
  - [2] E. J. Snijder and M. C. Horzinek, in *The Coronaviridae*, edited by S. G. Sidell, 219 (Plenum Press, New York, 1995)
  - [3] J. Liu, H. Dai, J. H. Hafner, D. T. Colbert, R. E. Smalley, S. J. Tans and C. Dekker, Nature **385**, 780 (1997).
  - [4] L. Liu, G.Y. Guo, C. S. Jayanthi and S.Y. Wu, Phys. Rev. Lett. **88**, 217206 (2002).
  - [5] R. Martel, H. R. Shea and P. Avouris, Nature **398**, 299 (1999).
  - [6] R. C. Haddon, Nature **388**, 31 (1997).
  - [7] A. Perez-Garrido, M. J. W. Dodgson, and M. A. Moore, Phys. Rev. B **56**, 3640 (1997).
  - [8] M. J. Bowick, D. R. Nelson and A. Travesset, Phys. Rev. B **62**, 8738 (2000).
  - [9] V. Vitelli, J. B. Lucks, and D. R. Nelson, Proc. Natl. Acad. Sci. USA **103**, 12323 (2006).
  - [10] L. Giomi and M. J. Bowick, Phys. Rev. B **76**, 054106 (2007);.
  - [11] B. I. Dunlap, Phys. Rev. B **46**, 1933 (1992); Phys. Rev. B **49**, 5643 (1994); Phys. Rev. B **50**, 8134 (1994).
  - [12] R. Saito, G. Dresselhaus and M. S. Dresselhaus, *Physical Properties of Carbon Nanotubes* (Imperial College Press, London, 1998).
  - [13] P. Lambin, A. Fonseca, J. P. Vigneron, J. B. Nagy and A. A. Lucas, Chem. Phys. Lett. **245**, 85 (1995); A. Fonseca, J. Hernadi, J. B. Nagy, P. Lambin and A. A. Lucas, Synth. Met. **77**, 249 (1996); V. Meunier, P. Lambin and A. A. Lucas, Phys. Rev. B **57**, 14886 (1998).
  - [14] Z. Yao, H. W. Ch. Postma, L. Balents and C. Dekker, Nature **402**, 273 (1999).
  - [15] S. Itoh, S. Ihara and J. I. Kitakami, Phys. Rev. B **47**, 1703 (1993); S. Ihara, S. Itoh and J. I. Kitakami, Phys. Rev. B **47**, 12908 (1993); S. Itoh and S. Ihara, Phys. Rev. B **48**, 8323 (1993).
  - [16] J. E. Avron and J. Berger, Phys. Rev. A **51**, 1146 (1995), J. Chem. Soc. Faraday. Trans. **91**, 4037 (1995).
  - [17] D. Mumford, *Tata Lectures on Theta I* (Birkhäuser, Boston, 1983); J. Polchinski, *String Theory*, Vol. I (Cambridge University Press, Cambridge, 1998).
  - [18] J. Han, Tech. Rep. NAS (1997); Chem. Phys. Lett. **282**, 187 (1998).
  - [19] D. R. Nelson, Nano Lett. **2**, 1125 (2002).